Photomodulation optical spectroscopy of CdHgTe graded band gap heterostructures

© O.S. Komkov[1], M.V. Yakushev[2]

[1] St. Petersburg Electrotechnical University „LETI“,
197022 St. Petersburg, Russia
[2] Rzhanov Institute of Semiconductor Physics, Siberian Branch, Russian Academy of Sciences,
630090 Novosibirsk, Russia

E-mail: okomkov@yahoo.com

Received August 24, 2023
Revised September 1, 2023
Accepted September 1, 2023

Multilayer mercury–cadmium–telluride photodetecting heterostructures grown by molecular beam epitaxy on Si and GaAs substrates were studied using the infrared photoreflectance method. Based on the period of Franz–Keldysh oscillations observed in the photoreflectance spectra, the strength of the built-in electric field near the „working layer — graded band gap near-surface layer“ heterointerface was determined in a contactless way. An analytical calculation of distribution of such field over the structure depth has specified the region in which the photomodulation signal is formed. The experimentally obtained field values turned out to be higher than the calculated ones, which is explained by the influence of the photovoltaic effect.

Keywords: photoreflectance, mercury–cadmium–telluride, MCT, CdHgTe, built-in electric field, Fourier transform infrared spectroscopy, Franz–Keldysh oscillations.

DOI: 10.61011/SC.2023.06.57160.33k

1. Introduction

The gradded band gap (varizonal) „mercury–cadmium–telluride“ heterostructures (MCT) were studied in this paper using infrared photoreflectance method [1]. Close attention has been paid to this solid solution for many decades, since it allows the creation of matrix and linear photodetectors with extremely high characteristics for obtaining thermal images in the spectral ranges 3–5 and 8–14 μm [2].

Currently, epitaxial layers $Cd_xHg_{1-x}Te$ are widely used for the manufacture of photoresistive and photodiode IR radiation receivers, near the surfaces of which varizonal areas with an increasing band gap to the surface are formed. The estimation of the maximum rate of surface recombination in the absence of a varizonal layer on the surface gave the value 10^5 cm/s. When using a surface varizonal layer with a value of $\Delta E_{gs} = E_{gs} - E_{g0} = 0.1$ eV (where E_{gs} — the width of the band gap on the surface of the structure, and E_{g0} — at the boundary with a homogeneous semiconductor layer) when at a temperature of 80 K, this component of the surface recombination rate will be suppressed to values ~ 1 cm/s, i.e. by 5 orders of magnitude [3].

Historically, one of the most popular optical methods of non-destructive testing of MCT is photoluminescence [4,5]. However, another optical method developed in this work — infrared photoreflectance (IR photoreflectance) — has a number of advantages. It allows studying excited states in semiconductor structures and optical transitions with a low oscillator strength [6]. This method implemented on the basis of the Fourier transform infrared spectrometer [1] has already proven itself well in the study of narrow band gap $A^{III}B^{V}$ materials and nanostructures based on them [7,8]. The contactless analysis of built-in electric fields performed using the IR photoreflectance method based on the Franz–Keldysh oscillations (FKO) observed in the spectra is of particular interest. Such an analysis is possible even in the case of fundamentally inhomogeneous electric fields, which were observed, for example, in δ-doped layers of GaAs [9]. It was shown in this work that both positive and negative electric fields in the signal generation region affect the formation of the photoreflectance signal.

Experiments on measuring IR photoreflectance of MCT structures were undertaken earlier [10]. The spectra were measured on a step-scan Fourier transform infrared spectrometer in a spectral range up to $\lambda = 20\,\mu$m, which made it possible to record not only $E_g(Cd_{0.23}Hg_{0.77}Te)$, but also lower-energy transitions associated, according to the authors, with transitions involving „impurities“. However, the appearance of the spectra published in that work (as in a later article by the same authors [11]) indicates the absence of the necessary phase correction and represents the IR photoreflectance module. Nevertheless, signals in the energy range above E_g observed at 200–290 K in a paper published around the same time by the same scientific group [12], were associated with FKO and the „field“ determined based on their period was in the range 4.4–5.0 kV/cm.

This work is aimed at calculating the distribution of the intensity of the built-in electric field and the potential over the depth of the photodetector graded band gap MCT structures, identifying the area of formation of the IR photoreflectance signal, as well as the correct experimental determination of the electric field averaged over this area.

Table 1. Electrophysical parameters of heterostructures $Cd_xHg_{1-x}Te$

Parameter	Heterostructure number			
	1	2	3	4
Material substrate	Si	Si	GaAs	GaAs
x_{CdTe}, mole fractions	0.222	0.221−0.222	0.221±0.002	0.225
N_D, cm^{-3}	$8.4 \cdot 10^{14}$	$4.9 \cdot 10^{14}$	$5.4 \cdot 10^{14}$	$2.5 \cdot 10^{14}$
μ_n, $cm^2/B \cdot c$	34 000	42 000	93 000	54 000

2. Samples and experimental procedure

Samples of MCT heterostructures were grown on silicon and gallium arsenide substrates by molecular beam epitaxy [13,14]. The use of these substrates is much cheaper than the use of crystal lattice matched CdZnTe substrates. The diameter of the Si substrate was 76.2mm, and the diameter of GaAs substrate was 50.8mm. Orientation of both types of substrates — (013).

A sequence of buffer layers consisting of a very thin ZnTe, a relatively thick CdTe and a lower varizonal MCT layer was first grown on the substrates. Next, a thick working MCT layer of constant composition with a thickness of $6.3-8.6\,\mu m$ (the values of x_{CdTe} are given in Table 1) and the upper varizonal MCT layer (thickness $0.3-0.4\,\mu m$) were grown. The composition of all MCT layers was controlled with very high accuracy *in situ* by ellipsometry [15].

Table 1 also shows electron concentrations and mobilities measured at liquid nitrogen temperature after annealing structures to fill vacancies. It can be seen that the structures (especially on the GaAs substrate) have large mobility, which indicates the high quality of the studied structures.

The IR photoreflectance spectra were measured using an experimental setup described in [1]. The setup was assembled on the basis of Vertex 80 research class Fourier transform infrared spectrometer. The MCT samples were placed in the vacuum of a nitrogen cryostat with windows made of clarified zinc selenide and cooled to a temperature of 79 K. The reflectance coefficient of the samples was photomodulated using a modulating laser beam of a gallium arsenide semiconductor laser diode with $\lambda = 809$ nm radiation. The reflectance of the probe IR radiation emitted from the Michelson interferometer of the Fourier transform infrared spectrometer was measured at the modulation frequency. The frequency of laser intensity modulation was 2.5 kHz, which required step-scan movement of the movable mirror of the Michelson interferometer to implement synchronous detection. After the interaction of the laser radiation with the sample, the scattered laser radiation was absorbed by a GaAs filter, and the IR probe beam reflected from the sample was recorded by a photovoltaic detector cooled with liquid nitrogen. The phase of the modulated reflectance signal was restored according to the original method described in [16].

3. Results and discussion

3.1. Theoretical calculations of the energy diagram and distribution of the built-in electric field

The gradient of the composition at the surface leads to a significant change in the width of the band gap (Figure 1, *a*). After the redistribution of the mobile charge carriers, the level corresponding to the electron output into vacuum bends, and this leads to a change in the energy band diagram (Figure 1, *b*). The potential distribution in the varizonal heterostructure will be calculated according to [3,17,18].

The Poisson equation for the narrow band gap part of the heterostructure under consideration (for the working area):

$$\frac{\partial^2 \phi_1}{\partial z^2} = \frac{qN_{D_1}}{\varepsilon_0 \varepsilon_1}\left[\exp\left(\frac{q\phi_1}{kT}\right) - 1\right], \qquad (1)$$

where N_{D_1} — the concentration of the dopant in a narrow-band semiconductor is approximately equal to the concentration of free charge carriers.

Boundary conditions for the working area:

$$1)\ z = -\infty, \quad \phi_1 = 0, \quad F_1 = -\frac{\partial \phi_1}{\partial z} = 0;$$

$$2)\ z = z_{k1}, \quad \phi_1 = \phi_{k1}, \quad \varepsilon_1 F_1 = \varepsilon_2 F_2,$$

where z_{k1} — coordinate of „working area−upper varizonal layer“ heteroboundary (for sample 1 $z_{k1} = 7.38\,\mu m$). At this heteroboundary $\varepsilon_1 = \varepsilon_2$, since solid solutions of the same composition are in contact. The boundary „CdTe — varizonal buffer MCT layer“ is chosen as the the origin of the coordinates z in this work.

It is not possible to obtain the potential distribution from (1) analytically, so we will consider the asymptotic solution of this equation. The potential in the narrow-band part of the heterostructure away from the heteroboundary is small: $|q\phi_1| \ll kT$. Then the exponent in (1) can be decomposed into Taylor's series:

$$\exp\left(\frac{q\phi_1}{kT}\right) \approx 1 + \frac{q\phi_1}{kT}.$$

Hence, the equation (1) in this approximation can be represented as

$$\frac{\partial^2 \phi_1}{\partial z^2} = \frac{qN_{D_1}}{\varepsilon_0 \varepsilon_1}\frac{q\phi_1}{kT}.$$

Let's assume that

$$L_{D_1} = \left(\frac{\varepsilon_0 \varepsilon_1 kT}{q^2 N_{D_1}}\right)^{1/2}$$

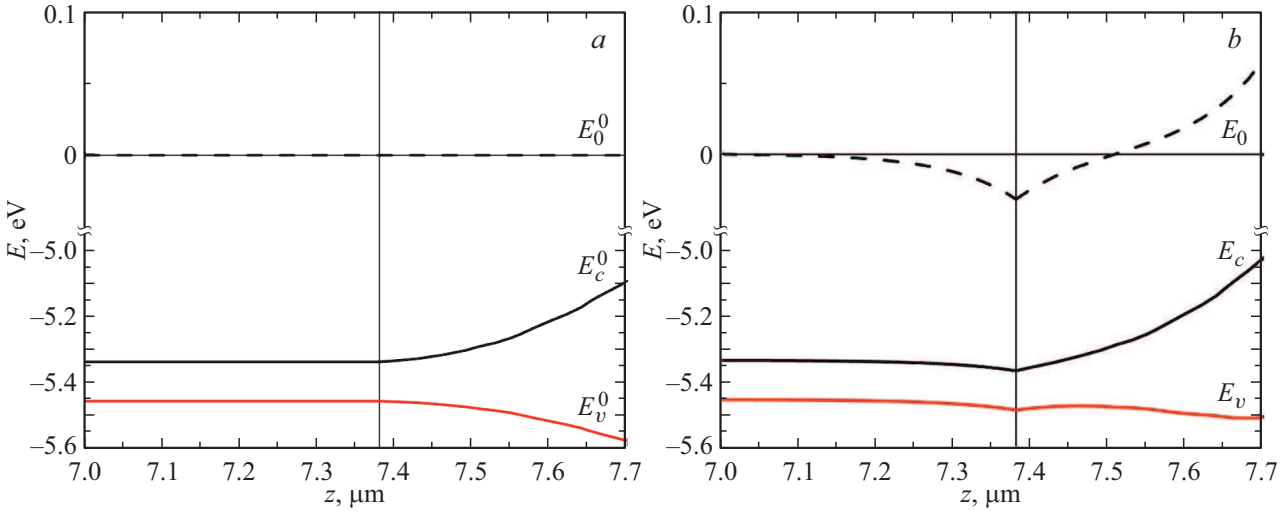

Figure 1. Energy diagram of a typical heterostructure $Cd_xHg_{1-x}Te$ (sample 1) near the interface before (a) and after (b) redistribution of mobile charge carriers (electrons).

— characteristic length, then

$$\frac{\partial^2\phi_1}{\partial z^2} - \frac{\phi_1}{L_{D_1}^2} = 0.$$

If we solve this equation using boundary conditions at $z = -\infty$ and $z = z_{k1}$, then we obtain

$$\phi_1(z) = \phi_{k1} \exp\left(\frac{z - z_{k1}}{L_{D_1}}\right). \qquad (2)$$

Thus, an approximate distribution of the potential in a narrow-band semiconductor away from the heteroboundary was obtained analytically.

We define the boundary conditions for the near-surface varizonal part of the heterostructure:

$$1)\ z = z_{k1}, \quad \phi_2 = \phi_{k1}, \quad F_1 = F_2;$$

$$2)\ z = z_{k2}, \quad \phi_2 = \phi_{k2}, \quad F_2 = -\frac{\partial\phi_2}{\partial z},$$

where z_{k2} — the boundary between the varizonal layer and the vacuum. For sample 1 selected to demonstrate the results $z_{k2} = 7.7\,\mu$m.

Let the 1st part of the varizonal region be at $z_{k1} \le z \le z_c$, where z_c — the coordinate at which the potential in the varizonal layer turns to zero. Then, according to [3], the solution of the Poisson equation for the first part of the varizonal layer will have the following form in the approximation of a linear change of composition and constancy ε

$$\phi_{21}(z) = \frac{\Delta E_c^0}{q} \frac{L_{D_1}}{z_{k2} - z_{k1}} \exp\left(-\frac{z_c - z_{k1}}{L_{D_1}}\right) \mathrm{sh}\left(\frac{z_c - z}{L_{D_1}}\right),$$

where $\Delta E_c^0 = E_c^0(z_{k2}) - E_c^0(z_{k1})$ and

$$z_c = z_{k2} - \left(\frac{z_{k2} - z_{k1}}{2} + \frac{L_{D_1}}{2} \ln\left(2 - \exp\left(-\frac{z_{k2} - z_{k1}}{L_{D_1}}\right)\right)\right).$$

For the sample 1 shown in Figure 1 $z_c = 7.51\,\mu$m.

Hence, the maximum value of the potential for the working area of the heterostructure in the expression (2)

$$\phi_{k1} = \phi_{21}(z_{k1}) = \frac{\Delta E_c^0}{q} \frac{L_{D_1}}{z_{k2} - z_{k1}} \exp\left(-\frac{z_c - z_{k1}}{L_{D_1}}\right) \mathrm{sh}\left(\frac{z_c - z_{k1}}{L_{D_1}}\right).$$

Let the 2nd part of the varizonal region be at $z_c \le z \le z_{k2}$. Then, according to [3],

$$\phi_{22}(z) = -\frac{\Delta E_c^0}{q} \frac{L_{D_1}}{z_{k2} - z_{k1}} \frac{\mathrm{sh}\left(\frac{z - z_c}{L_{D_1}}\right)}{\mathrm{ch}\left(\frac{z_{k2} - z_c}{L_{D_1}}\right)}.$$

In the future, it is possible to obtain the distribution of the potential energy of charge carriers in samples by multiplying the obtained potential distribution by the electron charge.

It is necessary to know the electron affinity energy for a solid solution of the MCT before the redistribution of free charge carriers near the heteroboundary to find the initial position of the bottom of the conduction band. Let the vacuum energy $E_0 = 0$ over the heterostructure, and the electron affinity energy is calculated by [19]:

$$\chi = 5.59 - 1.29x + 0.54x^2 - 0.56x^3 + 7.13 \cdot 10^{-4}Tx.$$

Then $E_c = E_0 - \chi$.

Currently, several dependencies are known $E_g(x, T)$, the most widely used expression for the band gap width is [20]:

$$E_g = -0.302 + 1.93x - 0.81x^2 + 0.832x^3 + 5.35 \cdot 10^{-4}(1 - 2x)T.$$

All calculations were performed for $T = 79\,\mathrm{K}$ — temperature according to the sensor installed in the used cryostat. The dielectric constant of the MCT material was determined by the formula from [21]:

$$\varepsilon = 20.5 - 15.6x + 5.7x^2,$$

where $x = x_{\mathrm{CdTe}}$.

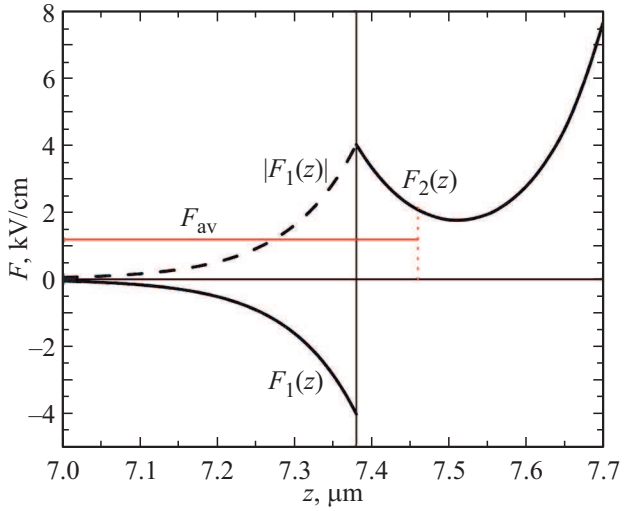

Figure 2. Distribution of the built-in electric field in the varison structure $Cd_xHg_{1-x}Te$ (thick solid curves), the field modulus in the working area (dashed line) and the field strength averaged over the photoreflectance signal generation area (thin horizontal line).

The obtained distribution of the potential energy of charge carriers for sample 1 is shown in Figure 1, where the initial (a) and equilibrium (b) dependences of the edges of the conduction band and the valence band on coordinates are shown.

After obtaining the expressions for the potential distribution, it is possible to calculate the desired distribution of the electric field near the heteroboundary [3]:

$$F_{21}(z) = -\frac{\partial \phi_{21}(z)}{\partial z} = -\frac{\Delta E_c^0}{q}\frac{1}{z_{k2}-z_{k1}}\exp\left(-\frac{z_c-z_{k1}}{L_{D_1}}\right)\mathrm{ch}\left(\frac{z_c-z}{L_{D_1}}\right),$$

$$F_{22}(z) = -\frac{\partial \phi_{22}(z)}{\partial z} = -\frac{\Delta E_c^0}{q}\frac{1}{z_{k2}-z_{k1}}\frac{\mathrm{ch}\left(\frac{z-z_c}{L_{D_1}}\right)}{\mathrm{ch}\left(\frac{z_{k2}-z_c}{L_{D_1}}\right)}.$$

Since the potential distribution in the narrow-band (working) region of the heterostructure in the approximation we have chosen has the exponential form (2), then the field strength will also change exponentially:

$$F_1(z) = F_{1k}\exp\left(\frac{z-z_{k1}}{L_{D_1}}\right),$$

where

$$F_{1k} = -\left(\frac{\partial \phi_{21}(z)}{\partial z}\right)_{z=z_{k1}},$$

i. e.

$$F_{1k} = -\frac{\Delta E_c^0}{q}\frac{1}{z_{k2}-z_{k1}}\exp\left(-\frac{z_c-z_{k1}}{L_{D_1}}\right)\mathrm{ch}\left(\frac{z_c-z_{k1}}{L_{D_1}}\right).$$

The distribution of the electric field of sample 1 is shown in Figure 2 by a solid thick line.

Table 2. Theoretical fields at the heteroboundary, calculated areas of photoreflectance signal generation and average value of field strength in these areas

Characteristics	Number of the MCT heterostructure sample			
	1	2	3	4
Field strength at the $\|F_k\|$ heteroboundary, kV/cm	4.02	4.46	5.82	4.2
Width of the IR photoreflectance signal generation area, μm	0.46	0.59	0.52	0.73
Average value of the field strength modulus near heteroboundary F_{av}, kV/cm	1.19	1.16	1.41	1.05

As already noted in the Introduction, both positive and negative electric fields in the signal generation region affect the formation of the photoreflectance signal. Thus, we will consider the intensity module of the built-in electric field (the thick dashed line in Figure 2 — the intensity module of the built-in electric field).

The photoreflectance signal is formed by a region of the MCT heterostructure with a band gap width close to the band gap width of the working area, i. e. E_g (the maximum of the IR photoreflectance signal is observed with this energy as will be shown below). In addition, signal generation obviously occurs where there is a modulated electric field. Table 2 shows the values of the maximum field strength at the heteroboundary and the values of the width of the IR signal formation region, as well as the values of the modulus of the calculated built-in electric field averaged over this region for all four MCT structures studied.

The graph of the average value of the field strength for sample 1 is shown in Figure 2 is a thin horizontal line, and the boundary of the IR photoreflectance signal generation region (where E becomes significantly larger than the E_g varizonal layer) is indicated by a vertical dotted line.

3.2. Results of IR photoreflectance measurement

Figure 3 shows the IR photoreflectance spectrum obtained by us from sample 1 at $T = 79$ K in the wavelength range of 7–16 μm. The IR photoreflectance spectra from the other three structures studied had the same lineshape and are not shown here. The oscillating signal at an energy below E_g seems to be associated with interference (as in previous studies of InSb homoepitaxial layers [1]). This signal is caused by photomodulation of the refractive index and it was used to estimate the thickness of GaAs homoepitaxial layers in [22]. In our opinion, the use of the IR photoreflectance method to solve such a problem — is redundant. It is advisable to use a simpler optical technique to measure the thickness of a single layer, as described, for example, in [23].

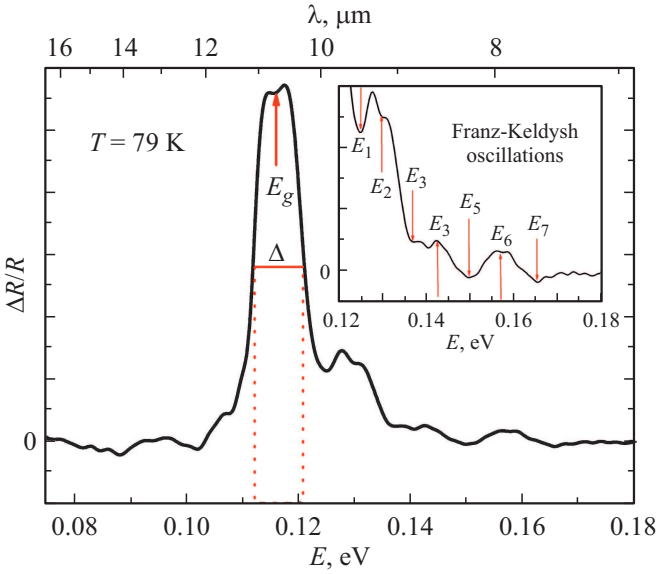

Figure 3. The typical IR photoreflectance spectrum of $Cd_xHg_{1-x}Te$ heterostructure with a varizonal near-surface layer. The insert shows the same spectrum on an enlarged scale.

The width at half-height (Δ) of the main peak can be a characteristic of the quality of the structure (the smaller it is, the better the quality). The values of Δ for all studied samples are summarized in Table 3. It also contains the values of E_g, which correlate well with the known composition of the working layer (see Table 1).

It is interesting to analyze the oscillating structure at an energy above E_g. Seven oscillations with energies (E_1–E_7) are clearly observed in the insert to Figure 3, representing the FKO indicated by the arrows.

When analyzing these oscillations according to the method described in [24], the experimental points as expected do not fit on one straight line (a similar situation was observed for δ-layers [9]). This is an experimental confirmation of the inhomogeneity of the built-in electric field, the calculation of the distribution of which over the thickness of the structure was carried out above.

The interband reduced effective mass in the direction of the field was calculated to estimate the intensity of F:

$$\frac{1}{\mu_{\|}} = \frac{1}{m_e^*} + \frac{1}{m_{hh}^*}.$$

The average effective mass of heavy holes in a solid solution of MCT $m_{hh}^* = 0.55m_0$ [21]. The effective mass of electrons in the MCT material is calculated as follows according to the same review:

$$\frac{m_0}{m_e^*} = -0.6 + \frac{19}{3}\left(\frac{2}{E_g} + \frac{1}{E_g + 1}\right).$$

The obtained values of $\mu_{\|}$ in units of free electron mass m_0 are listed in Table 3. The same table shows the desired experimental values of the averaged electric field F.

Table 3. The width of the peak of the IR photoreflectance at half-height, the width of the band gap, the interband reduced effective masses and experimentally measured values of the averaged electric field near the heteroboundary „working layer–varizonal layer“

Characteristics	Number of the MCT heterostructure sample			
	1	2	3	4
Δ, eV	0.009	0.009	0.010	0.006
E_g, eV	0.116	0.116	0.117	0.125
$\mu_{\|}/m_0$	0.0086	0.0086	0.0087	0.0092
F, kV/cm	3.4	3.9	3.2	3.4

Comparing the experimentally obtained values of the field strength F with the theoretical values F_{av} averaged over the IR signal generation region (see Table 2), it is clear that the experimental field is several times stronger than the theoretical one. This is explained by the additional illumination of the studied structures by modulating and probe IR rays, which generated additional photoinduced charge carriers. At the same time, the photovoltaic effect was not taken into account in the calculations.

4. Conclusion

Thus, the complex nature of the distribution of the built-in electric fields is theoretically obtained and their impct on the zone diagram of multilayer varizonal MCT structures is estimated. These fields at the interface „working area — upper varizonal layer“ lead to the formation of a triangular potential well for electrons (see Figure 1, *b*). Consequently, a conduction channel is formed along the varizonal MCT structure.

From the point of view of the development of the IR photoreflectance method, the studied structures are an interesting object with a fundamentally inhomogeneous built-in electric field. The FKO detected in them are formed in a non-trivial way. Both the region in which the built-in electric field is directed from the interface to the depth of the sample and the region with the field directed to the surface take part in the formation of oscillations. Modulation of these fields using an external IR laser made it possible to experimentally estimate the averaged intensity in the region near the interface, where the band gap of the sample is less than the energy of the probe beam. These experimentally measured fields turned out to be several times stronger than the calculated ones, which gives additional information about the structures in the conditions of external illumination. In addition, the values of the band gap of the working area of heterostructures were independently determined by the method of photomodulation optical spectroscopy, which will make it possible to clarify the actual composition of samples and their exact temperature during additional IR radiation.

Acknowledgments

The authors would like to thank A.I. Luferau and A. Tazhbenov for assistance in conducting measurements and calculations, respectively.

Conflict of interest

The authors declare that they have no conflict of interest.

References

[1] O.S. Komkov. Phys. Solid State, **63** (8), 1181 (2021).
[2] V.N. Ovsyuk, G.L. Kuryshev, Yu.G. Sidorov, V.V. Basovkin. *Matrichnye fotopriemnye ustrojstva infrakrasnogo diapazona* (Novosibirsk, Nauka, 2001). (in Russian).
[3] T.E. Kovalevskaya, V.N. Ovsyuk. Avtometriya, **40** (4), 57 (2004). (in Russian).
[4] M.S. Ruzhevich, K.D. Mynbaev. Rev. Adv. Mater. Technol., **2** (4), 47 (2020).
[5] M.S. Ruzhevich, K.D. Mynbaev. Rev. Adv. Mater. Technol., **4** (4), 17 (2022).
[6] K. Murawski, M. Kopytko, P. Madejczyk, K. Majkowycz, P. Martyniuk. Metrol. Meas. Syst., **30** (1), 183 (2023).
[7] M.Yu. Chernov, V.A. Solov'ev, O.S. Komkov, D.D. Firsov, A.D. Andreev, A.A. Sitnikova, S.V. Ivanov. J. Appl. Phys., **127** (12), 125706 (2020).
[8] D.D. Firsov, A.I. Luferau, D.V. Kolyada, M.Yu. Chernov, V.A. Solov'ev, A.D. Andreev, O.S. Komkov. J. Opt. Soc. Amer. B, **40** (2), 381 (2023).
[9] O.S. Komkov, R.V. Dokichev, A.V. Kudrin, Yu.A. Danilov. Tech. Phys. Lett., **39** (11), 1008 (2013).
[10] J. Shao, L. Chen, X. Lü, W. Lu, L. He, Sh. Guo, J. Chu. Appl. Phys. Lett., **95** (4), 041908 (2009).
[11] X. Chen, J. Jung, Zh. Qi, Liangqing Zhu, S. Park, Liang Zhu, E. Yoon, J. Shao. Optics Lett., **40** (22), 5295 (2015).
[12] J. Shao, X. Lü, Sh. Guo, W. Lu, L. Chen, Y. Wei, J. Yang, L. He, J. Chu. Phys. Rev. B, **80** (15), 155125 (2009).
[13] Y.G. Sidorov, S.A. Dvorestkiy, V.S. Varavin, N.N. Mikhailov, M.V. Yakushev, I.V. Sabinina. Semiconductors, **35** (9), 1045 (2001).
[14] M.V. Yakushev. Avtoref. dokt. dis. (Novosibirsk, Institute of Semiconductor Physics of SB RAS, 2011). (in Russian).
[15] K.K. Svitashev, V.A. Shvets, A.S. Mardezhov, S.A. Dvoretsky, Yu.G. Sidorov, E.V. Spesivtsev, S.V. Rykhlitsky, S.I. Chikichev, D.N. Pridachin. Avtometriya, **4**, 100 (1996). (in Russian).
[16] D.D. Firsov, O.S. Komkov. Tech. Phys. Lett., **39** (12), 1071 (2013).
[17] V.N. Ovsyuk. *Elektronnye processy v poluprovodnikah s oblastyami prostranstvennogo zaryada* (Novosibirsk, Nauka, 1984). (in Russian).
[18] O.S. Komkov. *Raschet poluprovodnikovyh geteroperekhodov* (St. Petersburg, Izd-vo SPbGETU „LETI“, 2018). (in Russian).
[19] A.V. Voitsekhovskii, D.I. Gorn, I.I. Izhnin, A.I. Izhnin, V.D. Goldin, N.N. Mikhailov, S.A. Dvoretskii, Yu.G. Sidorov, M.V. Yakushev, V.S. Varavin. Russian Physics Journal, **55** (8), 910 (2013).
[20] G.L. Hansen, J.L. Schmidt, T.N. Casselman. J. Appl. Phys., **53** (10), 7099 (1982).
[21] A. Rogalski. Rep. Progr. Phys., **68** (10), 2267 (2005).
[22] N. Kallergi, B. Roughani, J. Aubel, S. Sundaram. J. Appl. Phys., **68** (9), 4656 (1990).
[23] O.S. Komkov, D.D. Firsov, E.A. Kovalishina, A.S. Petrov. Russian Microelectronics, **44** (8), 575 (2015).
[24] A.N. Pikhtin, O.S. Komkov, K.V. Bazarov. Semiconductors, **40** (5), 592 (2006).

Translated by A.Akhtyamov